RESEARCH PAPER

# Synergistic nanomedicine: Catechin@Cerium-hydroxyapatite nanoparticles for oxidative stress mitigation and concurrent osteosarcoma ablation and Osteogenesis

*Panduranga Mounagurusamy Siva Subramanian[1], Lakshmi Pandian Ananthbalaji[2], Suriyan Sulochana[3], Christopher Joseph Kirubaharan[4], Thiru Selvan[5], Subramani Rajapandi[6*]*

*[1]SSM Institute of Engineering and Technology, Dindigul, India*
*[2]Department of Biotechnology, Erode Sengunthar Engineering College (Autonomous), Thudupathi, Erode, India*
*[3]Department of Chemistry, Christian College of Engineering and Technology, Oddanchatram, Dindigul, India*
*[4]Department of Chemistry, Rajalakshmi Institute of Technology, Poonamalle, Chennai, India*
*[5]Department of Forestry and Biodiversity, Tripura University (A Central University), Suryamaninagar, Agartala, Tripura, India*
*[6]Department of Chemistry, Erode Sengunthar Engineering College (Autonomous), Thudupathi, Erode, India*

**ABSTRACT**

***Objective(s):*** A significant problem in osteosarcoma treatment and bone regeneration is the creation of biomaterials that efficiently target cancer cells while concurrently facilitating bone tissue regeneration. We introduce an innovative dual-action nanomedicine, catechin-functionalized nano cerium-hydroxyapatite (CH@Ce-HA), aimed at addressing these constraints by integrating cytotoxic and regenerative capacity.

***Materials and Methods:*** The CH@Ce-HA composite was created by integrating the natural anticancer and antioxidant compound, catechin, onto a nanoscale cerium-doped hydroxyapatite matrix. The physicochemical analysis *via* FT-IR revealed the incorporation of catechin, while XRD validated the retention of the HA crystalline structure. TEM examination demonstrated a homogeneous distribution of nanoparticles ranging from 20 to 50 nm in size. The combined therapeutic efficacy was further examined *in vitro* utilizing osteosarcoma and osteoblast cell lines, evaluating cell proliferation, oxidative stress reduction, apoptosis induction, and osteogenic differentiation.

***Results:*** *In vitro* investigations utilizing osteosarcoma and osteoblast cell lines demonstrated the nanocomposite's exceptional therapeutic flexibility. The CH@Ce-HA demonstrated improved antioxidant activity and a strong nanomedicine effect against MG63 osteosarcoma cells, markedly suppressing proliferation, diminishing harmful oxidative stress, and effectively inducing apoptosis. The nanocomposite significantly improved osteoblast proliferation, differentiation, and mineralization.

***Conclusion:*** This study presents a potential, multifunctional ceramic based therapeutic agent that functions at the nanoscale to offer a comprehensive treatment for bone oncology. The CH@Ce-HA nanocomposite integrates targeted cytotoxic effects with robust osteogenic and antioxidant properties, marking a notable progress in translational nanomedicine treating challenging bone abnormalities and cancers.

***Keywords:*** *Osteosarcoma; Bone repair; Catechin; Osteoblast proliferation; Anti-oxidant activity*

**How to cite this article**

*Siva Subramanian PM, Ananthbalaji LP, Sulochana S, Kirubaharan CJ, Selvan Th, Rajapandi S. Synergistic nanomedicine: Catechin@Cerium-hydroxyapatite nanoparticles for oxidative stress mitigation and concurrent osteosarcoma ablation and Osteogenesis. Nanomed J. 2026; 13(3): 455-468. DOI: 10.22038/NMJ.2026.91797.2326*

## INTRODUCTION

Osteosarcoma is an extremely prevalent major malignant bone tumor, affecting young people during their growth years [1, 2]. In spite of the significant progress made in medical therapies and decades of research, osteosarcoma continues to pose a significant clinical challenge. Surgical resection of the tumor, frequently in conjunction with chemotherapy, and, in certain instances, radiation therapy, comprises the standard treatment regimen [3]. Nevertheless, these conventional methods have substantial drawbacks. Long-term survival rates of patients are still being impeded by chemoresistance, local recurrence, and

* *Corresponding author(s):* Subramani Rajapandi, PhD, Assistant Professor of Chemistry, Erode Sengunthar Engineering College (Autonomous),Thudupathi, Erode (District) 638 057, India. Phone: +91 9443400238, Email: rajapandichemistry@esec.ac.in.

Note. This manuscript was submitted on October 11, 2025; approved on April 26, 2026.

the propensity for distant metastasis, particularly to the lungs [4]. Additionally, osteosarcoma's aggressive nature frequently requires extensive surgical procedures, which may lead to extended recovery periods, functional impairment, and substantial bone loss [5]. The scientific community is increasingly utilizing nanotechnology to develop therapies that regenerate bone and target malignancy. This discipline provides innovative tools for enhancing drug delivery, improving the efficacy therapeutics, and mitigating side effects [6]. Nanoparticles (NPs) can be engineered to selectively target cancer cells, deliver medications more efficiently, and influence biological processes in a manner that conventional therapies cannot, due to their unique physicochemical characteristics [7].

Hydroxyapatite (HA) nanoparticles (NPs), which are inorganic components with a high surface area, have attracted considerable attention for their use in bone cancer research [8,9]. This bioactive ceramic material is an exceptional candidatefor coatings because of its biological suitability, bioactivity, osseointegration, non-toxicity, anti-inflammatory properties, osteoblast proliferation, osteoinduction, and osteoconductivity [10,11]. It also exhibits a strong affinity for pathogenic microbes, an acceptable ion exchange capacity with heavy metals, and the ability to establish chemical interactions with hard tissues [12]. In the past, HA has been employed as a restorative material to stimulate bone growth in cementless hip operations and non-weight-bearing procedures [13-15]. However, the inadequate antibacterial properties of HA constitute a significant drawback, as they may result in implant failure due to infection. In order to overcome this obstacle, the antibacterial resistance and physical properties of HA can be substantially enhanced by doping it with a diverse array of ions, including $K^+$, $Ag^+$, $Mg^{2+}$, $Zn^{2+}$, $Sr^{2+,}$ $Al^{3+}$, $In^{3+}$, $Y^{3+}$ elements, without altering its structure [10,16,17]. The antibacterial activity, biocompatibility, solubility, bioactivity, and overall stability of HA can be enhanced by subtly altering its properties, including glattice, crystallinity, and morphology, through ionic substitutions [18].

Cerium nanoparticles (CeNPs) are employed in biomedical applications to enhance the mechanical characteristics of bone, stimulate the formation of new bone, promote osteoblast proliferation, and exhibit antimicrobial properties [19, 20]. Cerium ions are present in two oxidation states**:** $Ce^{3+}$ and $Ce^{4+}$; the antibacterial and antioxidant properties of redox-active nanoceriaare attributed to the unique ability of $Ce^{2+}$ ions to transition between oxidation states [21]. The anticancer activity of CeNPs is characterized by the stimulation of apoptosis, the inhibition of angiogenesis, and the disruption of the cell cycle, in addition to their scavenging of ROS. These characteristics are essential for the prevention of tumor growth and metastasis [22-24]. The property of HA can be improved by incorporating cerium into an HA lattice, capitalizing on cerium's excellent anticorrosion characteristic [25,26]. The therapeutic efficacy of nanoparticle-based systems is being enhanced by the exploration of naturally occurring compounds that possess established anticancer and regenerative properties [27].

Catechins (CH), a naturally occurring antioxidant, were employed to surface functionalize Ce-HA and thereby enhance its osteoinductive and osteoconductive effects [28-31]. CH are well-known for their potent antioxidant, anti-inflammatory, and anticancer characteristics, implying that CH have significant potential for osteosarcoma therapy [32,33]. They possess the capacity to regulate critical cellular processes that are implicated in cancer, including angiogenesis (the formation of blood vessels), cell proliferation, and apoptosis (Programmed cell death). Additionally, polyphenols are advantageous for the treatment of osteosarcoma and the promotion of bone regeneration following surgery, as they have the ability to inhibit bone degradation and stimulate bone formation, and exert anticancer properties [34-36].

This study aims to create a novel, multifunctional bioactive composite by combining cerium-doped hydroxyapatite nanoparticles (NPs) with the natural antioxidant CH, leveraging their synergistic medicinal properties. The nanocomposite exhibited superior biocompatibility with healthy MC3T3-E1pre-osteoblasts, maintaining high cell viability (98%), while specifically targeting cancer MG63 cells. The primary objective is to examine the synergistic effects of the CH@Ce-HA composite, emphasizing its selective anticancer activity through the induction of mitochondrial dysfunction and apoptosis (through increased expression of caspases-3, -8, and -9, and modulation of the Bax/Bcl-2 ratio) in osteosarcoma cells. The research evaluates the composite's ability to expedite bone tissue regeneration by significantly increasing the mRNA expression of essential osteogenic markers (Runx2, OPN, ALP, and OCN, as validated by RT-PCR studies). The CH@Ce-HAnanocomposites concurrently promote bone tissue regeneration and healing, thereby addressing the challenges of treating osteosarcoma (Fig. 1).

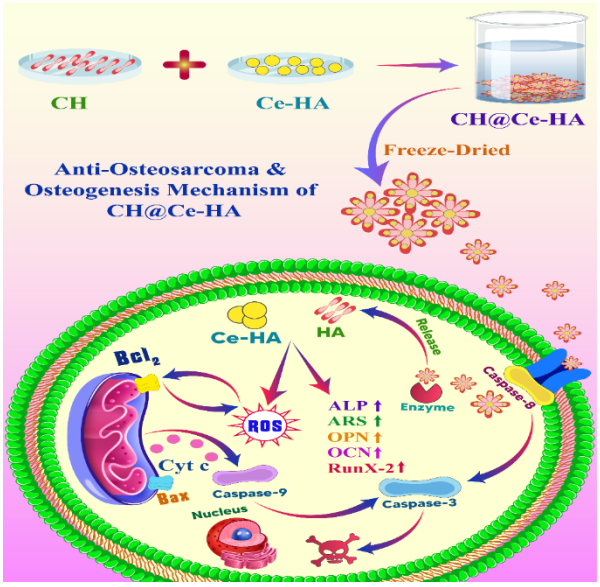


Fig. 1. Schematic representation of anti-osteosarcoma and osteogenesis mechanism of CH@Ce-HA.

## MATERIALS AND METHODS

### *Fabrication of Ce-HA nanoparticles*

The metal-doped HA NPs were produced *in situ* using a hydrothermal technique, adopted from published studies [37, 38]. The Ce-HA nanocomposite was created *via* a controlled precipitation technique, and subsequently underwent hydrothermal treatment. Initially, $Ca(NO_3)_2 \bullet H_2O$ and $Ce(NO_3)_3 \bullet 6H_2O$ precursors were mixed in a 0.8:0.2 molar ratio, while a 0.6 M solution of the phosphate precursor $(NH_4)_2HPO_4$ (Sigma Aldrich) was prepared separately. The essential procedure for nanoparticle synthesis included the gradual dropwise addition of a phosphate precursor solution to a $Ca^{2+}$: $Ce^{3+}$ mixture under constant stirring at RT, thereby initiating the *in-situ* precipitation of Ce-doped HA (Ce-HA) through the reaction of Ca and $PO_4^{2-}$ ions, while maintaining a Ca/P ratio of 1.67. The pH of the resulting suspension was promptly adjusted to 9 using 1 M NaOH. Then, the suspension underwent hydrothermal treatment at 200°C for 30 minutes in a microwave oven (MARS-5X) to facilitate the development and crystallization of the Ce-HA nanoparticles (NPs), which were then washed and dried at 100°C.

### *Fabrication of CH@Ce-HA nanocomposites*

The nanocomposites were prepared for biological experiments by combining 2% CH with Ce-HA NPs. The 2% catechin was dissolved in 10 ml of water**,** which was slowly added to the solution containing Ce-HA composites. The magnetic stirrer was used to continuously stir the mixture for 4 hours. The CH@Ce-HA nanocomposites were subsequently formed by freeze-drying the resulting suspension at -80°C under a pressure of 4 MPa. The final product was subsequently preserved at -4°C for future biological assays.

### *Characterization of the CH@Ce-HA nanocomposites*

X-ray diffraction examination was performed within the 2θ range of 10-75° to determine the crystalline structure of the hydroxyapatite powder (Malvern Panalytical instrument). FT-IR (Thermo Scientific) was utilized to confirm the chemical moieties present on the surface of the CH@Ce-HA nanocomposites, with spectra noted in the 400-4000 $cm^{-1}$ wavenumber range. The morphology, size, and dispersion of the Ce-HA and CH@Ce-HA nanocomposites were characterized using transmission electron microscopy (TEM).

### *Evaluation of antioxidant activity*

The antioxidant capacity was assessed via the ABTS test. Various concentrations of CH or CH@Ce-HA nanocomposites were combined with the ABTS working solution and peroxidase in a 96-well plate. Following 5-minute incubation, absorbance was determined at 414 nm. The following formula was employed to ascertain the scavenging rate.

ABTS (%) = [(Ab control – Ab sample) / Ab control] × 100%

### *Cell culture*

The human osteosarcoma cell lines (MG63) and osteoblastic cell lines (MC3T3-E1) were procured and propagated in DMEM enriched with 10% FBS and 1% antibiotics and α -MEM medium enriched with 2mM Glutamine and10% FBS. The cell cultures were all kept at 37°C in an atmosphere with 5% $CO_2$.

Table 1. RT-qPCR primers for the assessment of apoptosis related genes expression

| Gene | Forward | Reverse |
|---|---|---|
| β-actin | 5'-CTCTTTTCCAGCCTTCCTTC-3' | 5'-TCTCCTTCTGCATCCTGTC-3' |
| $BCL_2$ | 5'-GAGGATTGTGGCCTTCTTTG-3' | 5'-AGGTACTCAGTCATCCACA-3' |
| Cyt c | 5'-GAGATGAACAGGGGCTCGAAC-3′ | 5'-TGCTTCTGCCACATGATAACG-3′ |
| Bax | 5'-ATGGAGCTGCAGAGGATGA-3' | 5'-CCAGTTTGCTAGCAAAGTAG-3' |
| Caspase-8 | 5'-CATCCAGTCACTTTGCCAGA-3' | 5'-GCATCTGTTTCCCCATGTTT-3' |
| Caspase-9 | 5'-TTCCCAGGTTTTGTTTCCTG-3' | 5'-CCTTTCACCGAAACAGCATT-3' |
| Caspase-3 | 5'-GGACCTGTGGACCTGAAAAA-3' | 5'-CACTGTCTGTCTCAATACCG-3' |

***Cytotoxicity evaluation***

MG63 and MC3T3-E1 cells were inoculated at a density of $5 \times 10^5$ cells/well in a 96-well plate and incubated for 24 hrs in α-MEM at 37°C in an environment of 5% $CO_2$. Next, fresh α-MEM containing serially diluted CH@Ce-HA(25 to 125 µg/mL) was introduced to the culture medium. After 18 and 36 hrs, 20 µL of 5 mg/mL MTT solution was added to each well and cultured for 4 hrs. The formazan crystals were solubilised in 150 µL DMSO, and the absorbance was quantified at 570 nm using a microplate reader [39]. Following the MTT test results, a concentration of 125 µg/mL was chosen for further cellular and molecular investigations.

MG63 and MC3T3-E1 cells were subjected to a live/dead cell staining experiment in order to evaluate cytotoxicity. After being seeded in 48-well plates, the cells were exposed to DOX, CH, Ce-HA, and CH@Ce-HA for 24 hours. To distinguish between living and dead cells, Calcein-AM/PI staining was used. The data were acquired using an Olympus IX73 inverted fluorescence microscope.

***ROS detection***

Intracellular ROS production was assessed using the DCFH-DA fluorescent probe. MG63 cells were seeded in 12-well plates and treated with the samples for 24 hrs. Cells were then incubated with DCFH-DA and imaged using an Olympus IX73 inverted fluorescence microscope. For quantitative analysis, cells were harvested, incubated with DCFH-DA, and analysed using a fluorescent reader (excitation: 488 nm, emission: 525 nm).

***Assessment of MMP***

MMP was evaluated using the Rhodamine 123 fluorescent dye. MG63 cells were plated in 6-well plates at a concentration of $2 \times 10^4$ cells/well and were co-cultured with the samples for 24 h. After subsequent washing with PBS, MG63 cells were stained with Rhodamine 123 for 20 minutes to evaluate MMP. Fluorescence images were then obtained via an inverted fluorescence microscope.

***qRT-PCR examination of apoptosis-associated gene expressions***

The expression of apoptosis-related genes was examined by qRT-PCR after 36 hrs of co-culturing the cells with the samples. TRIzol reagent was employed to extract total RNA and SuperScript IV UniPrime reagent mix was utilized to conduct reverse transcription. The expression levels of caspase-3, Bax, caspase-8, Bcl-2, caspase-9, and cytochrome c were measured using a fluorescence qRT-PCR apparatus (Quant Studio Real-Time PCR Systems, Thermo Fisher Scientific) in conjunction with the Bio-Rad SYBR Green Master Mix. β-actin served as the normalization control, and gene expression was evaluated with the ΔCt technique. Table 1 lists the primer sequences for the genes.

***In vitro Osteogenic differentiation of MC3T3-E1 Cells***

To induce osteogenic differentiation, the culture medium was supplemented with osteogenic differentiation factors**,** including 50 µg/mL ascorbic acid, 10 mM β-glycerophosphate, and 100 nM dexamethasone. Cells were maintained under these conditions for up to 14 days, with medium replenished every 2-3 days and were also co-cultured with the samples.

ALP, an early osteogenic differentiation marker, was assessed on days 7 and 14 post-treatment. At these time points, cells were washed twice with phosphate-buffered saline (PBS) and fixed with cold 4% paraformaldehyde for 15 min at RT. After fixation, cells were rinsed with PBS and incubated with an ALP staining reagent (BCIP/NBT). The development of a blue/purple precipitate indicated ALP enzymatic activity. Stained cells were gently washed with PBS to remove excess stain and imaged under an inverted light microscope at 10x magnification.

To evaluate late-stage osteogenic differentiation and mineralization, calcium deposition was assessed using Alizarin Red S staining on days 7 and 14. After removal of the culture medium, cells were gently rinsed twice with PBS and fixed with 70% ethanol for 1 hour at RT. Following fixation, cells were stained with 2% Alizarin Red S solution (pH 4.2) for 30 min to specifically bind to calcium-containing mineralized nodules. Excess dye was removed by washing the cells multiple times with distilled water. Stained cultures were then visualized under a light microscope at 10x magnification. Red staining intensity and distribution indicated the degree of extracellular matrix mineralization [39].

Table 2. RT-qPCR primers for the assessment of osteogenic differentiation related genes expression

| Gene | Forward | Reverse |
|---|---|---|
| **GAPDH** | 5'-CTGAGAATGGGAAGCAGGTC-3' | 5'-GAAGGGGCAGAGATGATGAC-3' |
| **OCN** | 5'-CACACTCCATCTTCGTGCTC-3' | 5'-AACGCCAAAAGCCAAAGCC-3' |
| **OPN** | 5'-TGCAAACACCGTTGTAACCAAGC-3' | 5'TGCAGTGGCCGTTTGCATTTCT-3' |
| **ALP** | 5'-TGCCTACTTGTGTGGCGTGAA-3' | 5'-TCACCCGAGTGGTAGTCACAATG-3' |
| **Runx-2** | 5'-TCTTCTGTCCATCCCTCTCC-3' | 5'-ACCCACATTCTGCCTTCCTC-3' |

***qRT-PCR evaluation of osteogenic genes***

After 14 days of incubation, total RNA was isolated from the cultured cells. The complementary DNA (cDNA) was synthesized from the isolated RNA using a commercial cDNA synthesis kit method. qRT-PCR was then performed to assess the expression levels of osteogenic genes, including ALP, OCN, OPN, and Runx2. Gene expression levels were normalized to GAPDH, which served as the internal control (Table 2).

***Statistical analysis***

Data are shown as mean ± SD. Group data was compared using Student's t-test. Statistical significance is indicated by * P < 0.05, ** P < 0.01, *** P < 0.001, **** P < 0.0001 using GraphPad Prism.

## RESULTS AND DISCUSSION

***Characterization of Ce-HA and CH@Ce-HA nanocomposites***

XRD examination of Ce-HA and CH@Ce-HA samples confirmed the effective synthesis of both materials (Fig. 2a). The distinctive diffraction peaks of pure HA (JCPDS no. 09-0432) were seen in both spectra, validating the establishment of the apatite structure [40]. The XRD pattern of Ce-HA and CH@Ce-HA nanocomposites displayed additional diffraction peaks corresponding to the crystalline planes (311), (220), (200), and (111) of Ce (JCPDS no. 81-0792) [41], indicating the successful integration of cerium into the apatite lattice. Furthermore, subdued peaks in the 2θ region of 16–28° indicated the presence of catechin, corroborating prior research on nanoparticle-organic chemical conjugates [42]. The exceptional purity of the produced materials and the lack of notable impurities were confirmed by the absence of extra peaks in the XRD patterns Ce-HA and CH@Ce-HA.

The FT-IR studies of Ce-HA and CH@Ce-HA nanocomposites were examined to assess the chemical composition and interactions among the components. The spectra of Ce-HA exhibited characteristic absorption bands at 3481 $cm^{-1}$ and 1030 $cm^{-1}$, corresponding to the vibrational modes of structural OH and phosphate groups (Fig. 2b). These bands signify the development of the apatite structure. The FT-IR spectra of CH showed broad absorption bands at 3417 $cm^{-1}$ assigned to OH stretching of phenolic groups, and a band at 1330 $cm^{-1}$, corresponding to in-plane bending vibrations [43, 44].

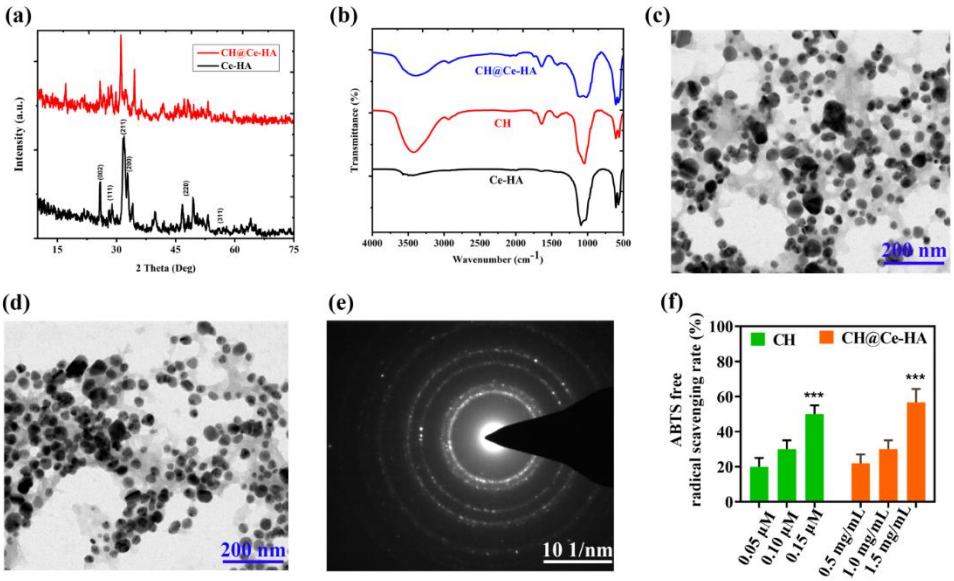


Fig. 2. (a) XRD Patterns of Ce-HA and CH@Ce-HA nanocomposites, (b) FT-IR Spectra of CH, Ce-HA, and CH@Ce-HA nanocomposites, (c) TEM image of Ce-HA, (d)TEM image of CH@Ce-HA(e) SAED image of CH@Ce-HA (f)% of ABTS free radical scavenging activity of CH and CH@Ce-HA nanocomposites.

Furthermore, the C=C stretching of aromatic rings and C-O/C-C stretching vibrations were ascribed to bands in the 1600-1400 $cm^{-1}$ and 1300-1200 $cm^{-1}$ regions, respectively. In comparison to pure Ce-HA, the CH@Ce-HA nanocomposites exhibited additional absorption bands at 1437 $cm^{-1}$ and 1322 $cm^{-1}$, indicative of the C-C stretching vibrations of aromatic rings from the CH moiety. The presence of these new bands suggests effective integration of CH into the Ce-HA lattice and indicates the development of a chemical interaction between the Ce-HA surface and CH, potentially through hydrogen bonding between the hydroxyl groups of Ce-HA and phenolic groups of CH. The biocompatibility of the CH@Ce-HA nanocomposites may be enhanced by these interactions, rendering them promising candidates for a variety of biological purposes.

The HR-TEM was employed to examine the crystalline structure and morphology of the Ce-HA and CH@Ce-HA nanocomposites (Fig. 2c&d). Both materials exhibited a predominantly spherical shape as evidenced by the HR-TEM images. The crystalline structure of CH@Ce-HAnanocompositeswas confirmed by the selected area electron diffraction (SAED) pattern (Fig. 2e). The overall spherical shape of the CH@Ce-HAnanocompositeswasnot significantly influenced by the inclusion of CH on their surface. Nonetheless, a little augmentation in particle size and possible alterations in the crystalline structure resulting from the interaction with CH are conceivable. The findings suggest the integration of CH into the Ce-HA lattice may alter the physical characteristics of the nanocomposite, possibly impacting its biocompatibility and bioactivity.

### *ABTS free radical scavenging ability of Ce-HA and free CH*

The antioxidant ability of CH and the CH@Ce-HA nanocomposites was assessed using the ABTS free radical scavenging test. Fig. 2f demonstrates that both free CH and CH@Ce-HA nanocomposites had similar ABTS free radical scavenging capacities, achieving about 63% and 59% inhibition, respectively, at the maximum doses tested. A concentration-dependent enhancement in the rate of free radical scavenging was noted for both CH (0.05 µM to 0.15µM) and CH@Ce-HA nanocomposites (0.5 mg/mL to 1.5 mg/mL), indicating that the conjugation of CH to the CH@Ce-HA nanocomposites surface did not negatively affect its intrinsic antioxidant properties. The design of catechin-loaded Ce-HA NPs preserves the inherent antioxidant capabilities of catechin, mitigating potential degradation caused by formulation, as indicated in the literature [45]. The maintenance of the biological activity of CH after its conjugation to the Ce-HA nanoparticle is essential for improving the therapeutic effectiveness of CH in bone-related disorders. The findings indicate that CH@Ce-HA maintains the antioxidant properties of free CH, thereby emphasizing its potential for the effective therapy of bone diseases. The antioxidant activity of CH, a primary bioactive component, has been extensively studied and is attributed to its iron-chelating effects and radical-scavenging capabilities. The therapeutic effectiveness of CH in bone-related disorders can be enhanced by conjugating it with Ce-HA NPs, as CH@Ce-HA nanocomposites maintain the antioxidant properties of the unbound molecule.

### *Assessment of cell viability in MG63 cells and MC3T3-E1 cells*

The cytotoxic profile of the DOX, CH, Ce-HA**,** and CH@Ce-HA nanocomposite exhibited an optimal therapeutic window, preferentially attacking cancer cells while preserving healthy tissue.The bar graph analysis of biocompatibility and dose-dependent cytotoxicity of the CH@Ce-HA nanocomposite was meticulously evaluated using an MTT test on MG63 osteosarcoma cells (Figure 3a) and healthy MC3T3-E1 pre-osteoblasts(Figure 4a)throughout a concentration range of 0 to 125 µg/mL. The findings revealed a markedly enhanced and selective cytotoxic profile in125 µg/mL CH@Ce-HA, showing significantly elevated toxicity towards the MG63 cells (up to 83.65% inhibition at elevated dosages) in contrast to free CH (42.31% inhibition) and Ce-HA (60.57% inhibition). The amplified inhibitory impact indicates that CH functionalization significantly enhances Ce-HA cytotoxicity, perhaps due to increased cellular uptake or synergistic intracellular interactions, potentially involving the generation of ROS within cancer cells. At this optimal concentration, the nanocomposite preserved the survivability of healthy MC3T3 pre-osteoblasts at around 98%, demonstrating exceptional biocompatibility. Microscopic images confirmed these results, revealing significant morphological damage (shrinkage, detachment, and fragmentation) in treated MG63 cells (Figure 3b), in stark contrast to the healthy, confluent morphology seen in treated MC3T3- E1 cells (Figure 4b). Importantly, the $IC_{50}$ values in the MG63 cell line are DOX – 39.5 µg/mL, CH – 53.2 µg/mL, Ce-HA – 52.0 µg/mL, and CH@Ce-HA – 46.8 µg/mL.The marked selective cytotoxicity towards MG63 cells is crucial, as it suggests that the CH@Ce-HA nanocomposite may improve targeted therapy delivery to malignant osteosarcoma cells while significantly reducing off-target detrimental effects on adjacent healthy bone tissues.

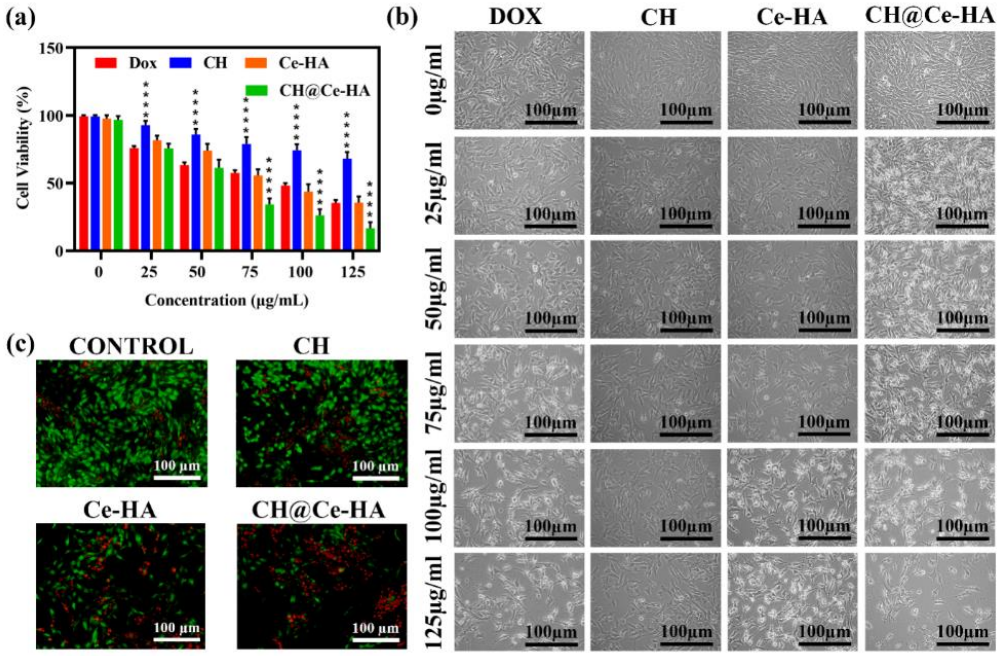


Fig. 3. **(a)** Assessment of dose-dependent cytotoxicity of DOX, CH, Ce-HA, and CH@Ce-HA nanocomposites on MG63 osteosarcoma cells for 24 hours and evaluated concentration range of 0 to 125 µg/mL using an MTT assay. Statistical annotations indicate significant differences (*p < 0.05, **p < 0.01, ***p < 0.001, ****p < 0.0001). **(b)** Representative bright-field microscope images of MG63 cells following 24 hrs of treatment with increasing doses. (Magnification: 20x). **(c)** Live/Dead analysis of MG63 cells in treated groups for 24 hrs and stained using Calcein AM/PI assay. (Scale bar: 100 µm).

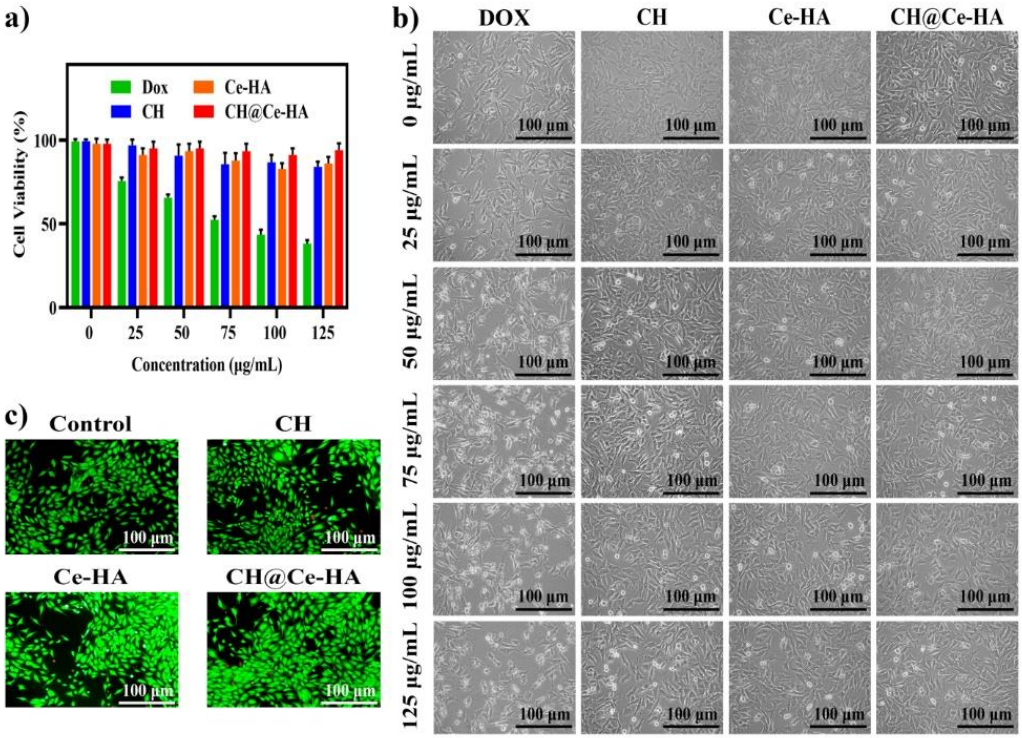


Fig. 4. **(a)** Assessment of dose-dependent cell viability of DOX, CH, Ce-HA, and CH@Ce-HA nanocomposites on MC3T3-E1 cells for 24 hrs and evaluated concentration range of 0 to 125 µg/mL*via* an MTT assay. Statistical annotations indicate significant differences: *p < 0.05, **p < 0.01, ***p < 0.001, ****p < 0.0001. **(b)** Representative bright-field microscope photos (magnification: 20x) of MC3T3-E1 cells following 24 hrs of treatment with escalating doses. **(c)** Live/Dead examination of MC3T3-E1 cells in treated groups using Calcein AM/PI assay. Scale bar: 100 µm.

***Live/Dead staining of CH, Ce-HA, and CH@Ce-HA nanocomposites***

The Live/Dead staining validated the distinct and enhanced cytotoxic effectiveness of the produced nanocomposite. Untreated MG63 cells demonstrated a viability rate of approximately 95% (shown by green fluorescence), thus providing a baseline for healthy cells. Although individual treatments with CH and Ce-HA resulted in only a slight reduction in MG63 cell viability, reflecting their low intrinsic cytotoxicity, the CH@Ce-HA nanocomposite exhibited a substantial decrease in viability, demonstrating the highest percentage of PI-positive (red, dead/late apoptotic) cells among all treatment groups (Figure 3c). The significant enhancement in cytotoxicity indicates a synergistic effect between CH and Ce-HA, likely due to improved cellular uptake of the functionalized material and a combined mechanism that involves the production of ROS, resulting in effective apoptosis induction in malignant cells. The CH@Ce-HA nanocomposite demonstrated maintaining the high viability (> 98%) of healthy MC3T3-E1 pre-osteoblasts compare to other treated groups (Figure 4c). This selectivity is crucial for clinical application, supporting CH@Ce-HA as a promising customized nanomedicine for localized osteosarcoma treatment with minimized off-target effects. The anti-osteosarcoma efficacy of CH@Ce-HA nanocomposites is substantially supported by the Live/Dead staining assay [50].

***Reactive oxygen species staining utilizing DCFH-DA on MG63 cells***

To investigate the function of ROS in CH@Ce-HA nanocomposites mediated apoptosis, the intracellular ROS levels were measured using the DCFH-DA fluorescent probe. The results indicated a substantial increase in ROS levels in cells treated with CH@Ce-HAin comparison to those in the Ce-HA and CH groups (Fig. 5a). The mild fluorescence intensity of untreated MG63 cells indicated a baseline concentration of intracellular ROS. Cells that were exposed to CH exhibited a slight increase in ROS levels, suggesting that it may induce oxidative stress. Analogous to CH, Ce-HA nanoparticles therapy induced a modest elevation in ROS levels. A markedly elevated quantity of ROS was detected in cells treated with CH@Ce-HArelative to the other groups, indicating a more intense oxidative stress response. The findings indicate that all three treatments (CH, Ce-HA, and CH@Ce-HA nanocomposites) stimulate ROS formation in MG63 cells, albeit the extent of ROS creation differs (Fig. 5b). Ce-HA also stimulated some ROS generation, maybe owing to its interaction with cellular components or the release of cerium ions. CH functionalization may enhance Ce-HA absorption, hence augmenting its accessibility to intracellular targets and facilitating ROS formation [46]. The data indicate that ROS-mediated pathways improve the cytotoxic effects of CH@Ce-HA nanocomposites on osteosarcoma cells relative to the individual components.

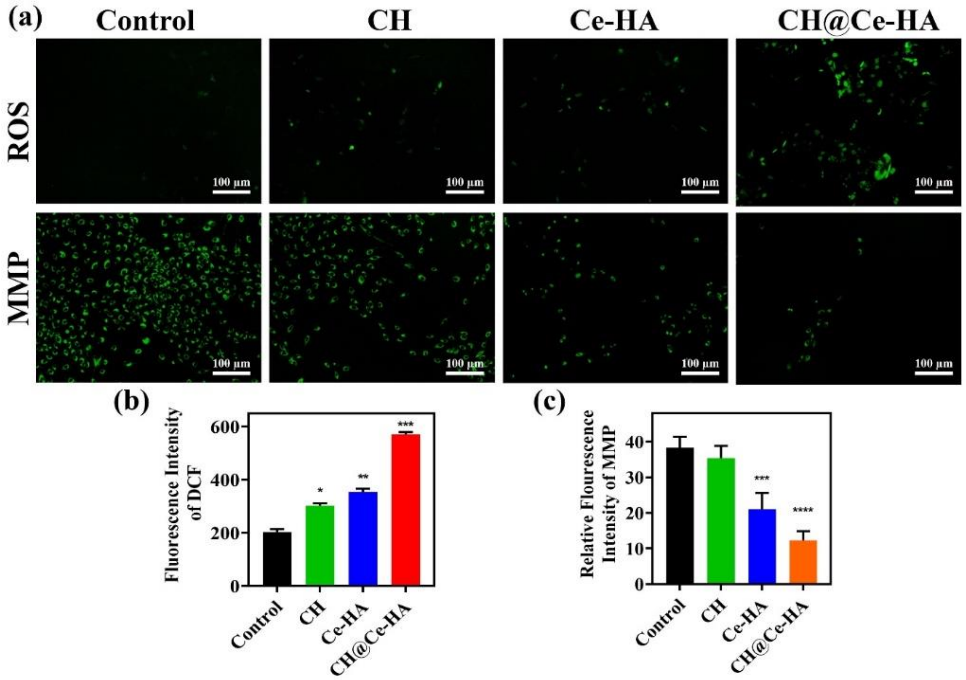


Fig. 5. **(a)** Intracellular ROS levels assessed using DCFH-DA fluorescence imaging and MMP assessed using Rhodamine 123 fluorescence imaging after various treatments (magnification: 20x, scale bar: 100 µm). **(b)**Flourescence Intensity of DCFH-DA. **(c)** Relative fluorescence intensity of MMP. Data are presented as mean ± SD, with statistical significance indicated as: *p < 0.01, **p < 0.001, ***p < 0.0001, ****p < 0.00001.

***Mitochondrial dysfunction and apoptosis induced by CH@Ce-HA nanocomposites in osteosarcoma cells***

The effect of CH@Ce-HA nanocomposites on mitochondrial function was measured by Mitochondrial Membrane Potential (MMP) using Rhodamine 123(Fig. 5a and c). A substantial reduction in green fluorescence, indicating mitochondrial depolarization, was seen in CH@Ce-HA nanocomposites-treated cells relative to controls. The results indicate that CH@Ce-HA nanocomposites cause a specific modification in mitochondria associated with cell death mechanisms. Dysfunctional mitochondria are integral to the intrinsic apoptosis mechanism. ROS produced by mitochondria or their interactions may increase mitochondrial permeability, resulting in the release of Cyt C into the cytosol. Cyt C initiates the caspase cascade, precipitating programmed cell death. The detected mitochondrial depolarization in CH@Ce-HA nanocomposites-treated cells indicates that nanocomposites may trigger apoptosis by disrupting mitochondrial function and facilitating Cyt C release. By activating pro-apoptotic proteins, including Bax and Bak, ROS can cause injury to mitochondria by opening the mPTP. The cellular metabolism and survival are impaired as a result of the decreased ATP production that results from this mitochondrial dysfunction [47, 48].

***Molecular mechanisms of apoptosis induced by* CH@Ce-HA*in osteosarcoma cells***

qRT-PCR was used to evaluate the expression of important apoptotic genes in order to elucidate the molecular processes of CH@Ce-HA nanocomposites-induced apoptosis. The findings suggested that CH@Ce-HAtherapy significantly increased the expression of caspases-3, -8, and -9, upregulated the pro-apoptotic gene Bax, and significantly decreased the anti-apoptotic gene Bcl-2. Additionally, the release of CytC, a defining indicator of apoptosis, was observed (Fig. 6). The data suggest that CH@Ce-HAinduces apoptosis through a multifaceted interaction with molecular pathways. It is likely that the upregulation of Bax and downregulation of Bcl-2 contribute to the generation of Cyt C and mitochondrial impairment. The initiation of the apoptotic cascade is indicated by the activation of caspases-3, -8, and -9. The observed modifications in gene expression suggest that both intrinsic and extrinsic apoptotic mechanisms are involved.

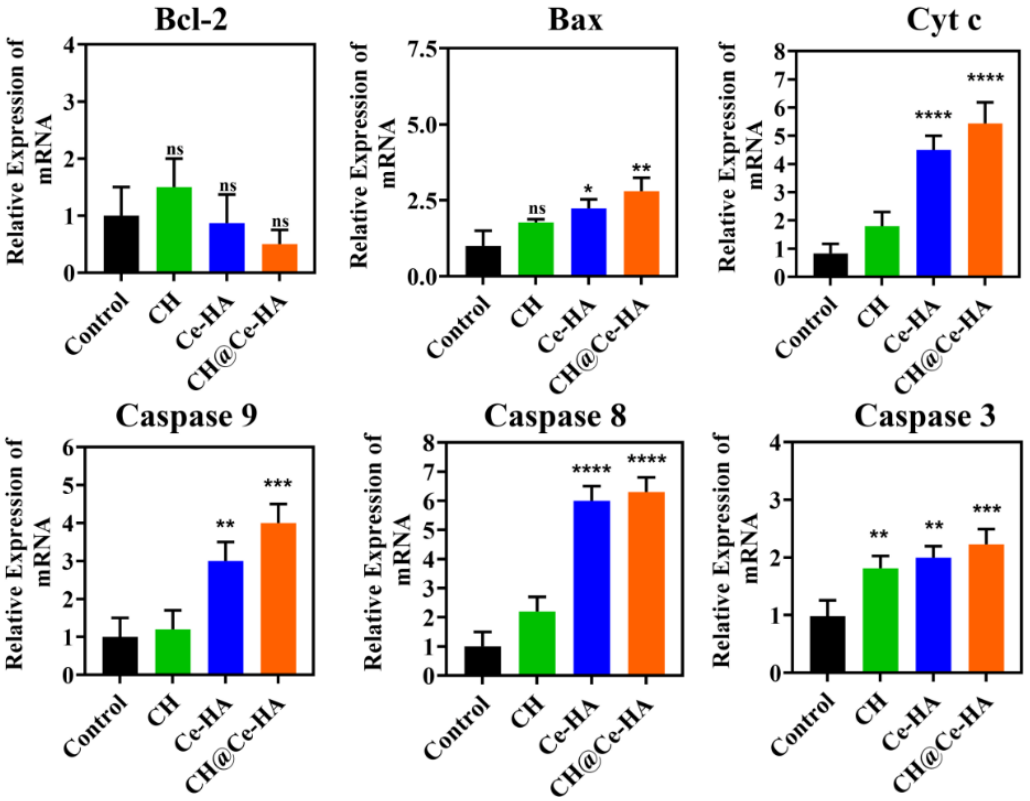


Fig. 6. RT-PCR quantification of apoptotic markers (Bcl-2, Bax, Cyt c, Caspase 9, Caspase 8, and Caspase 3). Data are presented as mean ± SD. Statistical significance is indicated as follows: *p < 0.05, **p < 0.01, ***p < 0.001, ****p < 0.0001.

The activation of both death receptor-mediated and mitochondrial-mediated apoptosis is indicated by the increased production of caspases-3, -8, and -9. The release of CytC and mitochondrial dysfunction can result from the the upregulation of Bax and downregulation of Bcl-2. This can initiate a cascade of events that ultimately activates caspase-3 by activating APAF-1 and caspase-9 [49]. The current investigation suggests that CH@Ce-HA nanocomposites activate both the intrinsic and extrinsic apoptotic pathways in osteosarcoma cells, thereby inducing apoptosis. The onset of apoptosis is consistent with the changes in gene expression, which are characterized by the upregulation of Bax and downregulation of Bcl-2, and activation of caspases. Apoptosis may be facilitated by the pro-oxidant properties of CH@Ce-HA nanocomposites

***Osteogenic differentiation in MC3T3-E1 cells***

ALP studies revealed that the CH@Ce-HA nanocomposite markedly enhances the initial stage of osteogenic differentiation in MC3T3-E1 pre-osteoblast cells (Fig. 7a). This enhancement was validated by a markedly increased accumulation of ALP activity**,** a vital, early-stage indicator of osteoblast commitment at both 7 and 14 days relative to the control. The significant rise in ALP activity indicates that the nanocomposite effectively facilitates the initial commitment and development of the osteoblast phenotype, underscoring its potential to expedite the osteogenic differentiation process for efficient bone regeneration.

To evaluate the osteogenic potential of CH@Ce-HA, the cells were cultivated for 7 and 14 days and then stained with Alizarin Red S, a dye that binds to calcium deposits (Fig. 7b). The control and CH groups had slight red staining, suggesting low calcium accumulation. Conversely, cells subjected to Ce-HA and CH@Ce-HA had differing levels of ARS staining, indicating a promotive influence on osteogenesis. Significantly, CH@Ce-HA nanocomposites exhibited the most robust osteogenic activity, presumably owing to the synergistic interaction between CH and Ce-HA.

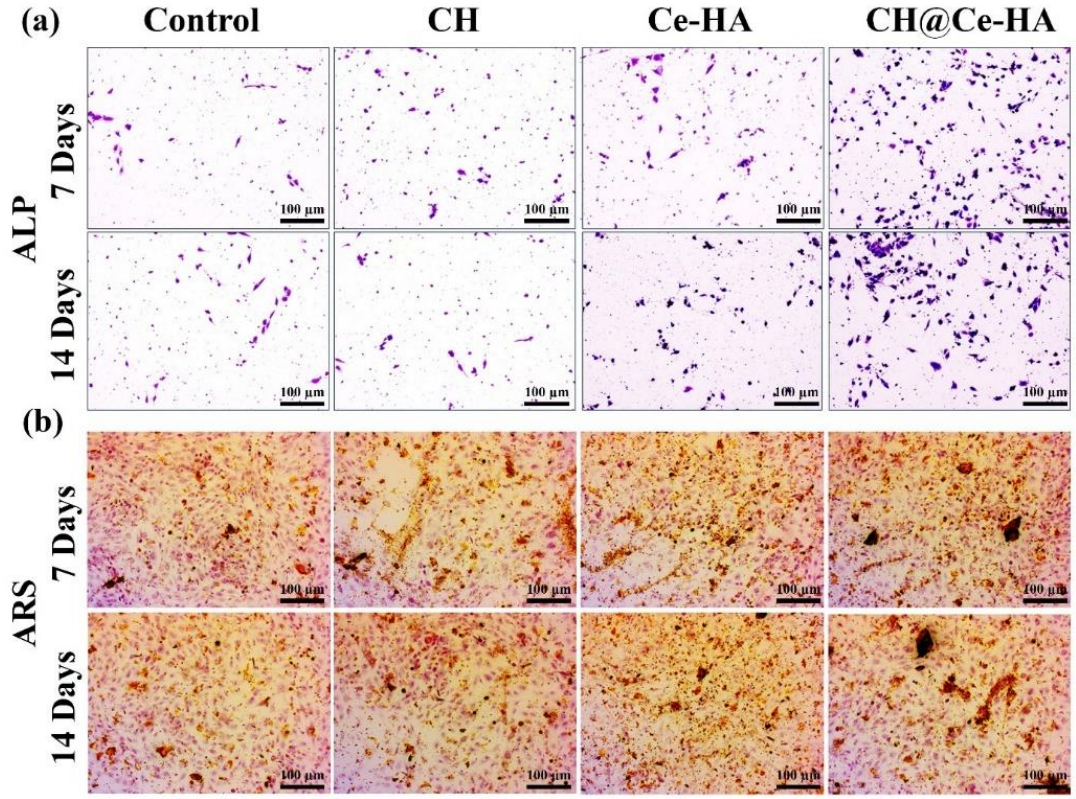


Fig. 7. **(a)** ALP staining of MC3T3-E1 cells at 7 and 14 days, indicating ALP activity. **(b)** Mineralization assessment at 7 and 14 days shows extracellular matrix mineral deposition. Images were taken at 10x magnification; scale bar: 100 µm.

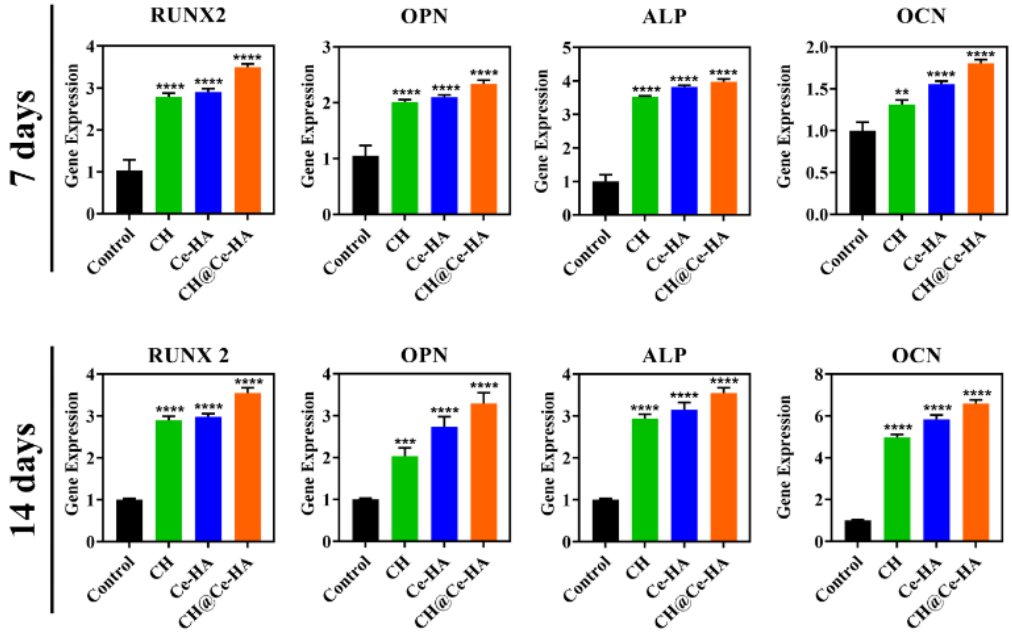


Fig. 8. Effect of CH@Ce-HA on osteogenic gene expression in MC3T3-E1 cells. Data are presented as mean ± SD, with statistical significance indicated as: *p < 0.05, **p < 0.01, ***p < 0.001, ****p < 0.0001.

The essential mechanisms regulating the observed cellular differentiation were elucidated through the analysis of major osteogenic gene expression via qRT-PCR (Fig.8). The CH@Ce-HA nanocomposites significantly increased the expression of all assessed markers, indicating an accelerated commitment to the osteoblast pathway. By Day 7, a notable increase of the master osteogenic transcription factor, Runx2, and the early commitment marker, ALP, was observed, signifying a fast induction of differentiation. By Day 14, the expression levels of Runx2 and ALP continued to be significantly raised, while a marked increase was also noted in the intermediate marker OPN and the late-stage mineralization marker OCN [50]. The concurrent elevated expression of Runx2 (promoting differentiation), ALP (indicating matrix maturation), and OCN (commencing mineralization) strongly indicates that the CH@Ce-HA nanocomposite not only initiates but also effectively advances the MC3T3-E1 cells through the phases of osteogenic development, resulting in improved bone matrix variation. These studies highlight the significant potential of this CH@Ce-HA nanocomposite as a suitable material for regenerative medicine and bone tissue engineering.

## CONCLUSIONS

This study investigated the effectiveness of catechin-functionalized nano-cerium hydroxyapatite (CH@Ce-HA) nanocomposite as a novel treatment for osteosarcoma. The results suggest that CH@Ce-HAexhibits increased cytotoxicity against MG63 osteosarcoma cells in comparison to free CHand Ce-HA when used independently. The synergistic interaction between CH and Ce-HA is likely the cause of the increased cytotoxicity. The increased generation of ROS leads to oxidative stress and apoptosis. Mitochondrial dysfunction, Cyt C release, and caspase activation. Through a synergistic activation of intrinsic and extrinsic apoptotic mechanisms, CH@Ce-HAtreatment induced apoptosis in MG63 cells. This effect was characterized by the upregulation of the pro-apoptotic gene Bax and the downregulation of the anti-apoptotic gene Bcl-2, which resulted in mitochondrial dysfunction. The initiation of the apoptotic cascade is indicated by the activation of caspases-3, -8, and -9. It is noteworthy that CH@Ce-HAdid not demonstrate any cytotoxicity toward healthy MC3T3-E1 cells, which indicates that it has the potential to be delivered to cancer cells in a targeted manner while simultaneously reducing adverse effects. This research suggests that CH@Ce-HAnanocomposites may be a viable therapeutic approach for the treatment of osteosarcoma.

## AUTHOR CONTRIBUTIONS

**P.S** –Conceptualization, Data curation, Methodology, Validation, Visualization, Writing – original draft, Writing – review & editing; **L.P.A** – Conceptualization, Data curation, Visualization, Writing – original draft, Writing – review & editing; **S.S** – Data curation, Validation, Visualization,

Writing – original draft, Writing – review & editing; **C.J.K**– Conceptualization, Data curation, Visualization, Writing – original draft, Writing – review & editing; **T.S**– Conceptualization, Data curation, Visualization, Writing – original draft, Writing – review &editing; **S.R**– Conceptualization, Data curation, Formal analysis, Funding acquisition, Investigation, Methodology, Supervision, Validation, Writing – original draft, Writing – review & editing.

## DATA AVAILABILITY

The datasets generated during the current study are available from the corresponding author on reasonable request.

## FUNDING

The authors declare that no financial support or external funding was received for the conduct of this research, authorship, and/or publication of this article.

## ACKNOWLEDGEMENT

The authors gratefully acknowledge Erode Sengunthar Engineering College (Autonomous), Erode, Tamil Nadu, India - 638057, for providing the laboratory facilities and infrastructure support necessary to carry out this research.

## CONFLICT OF INTERESTS

We declare that the authors have no competing interests.

## REFERENCES

1. Hosseini S, Sharifi E, Haghiralsadat BF, Mohsen SZ, Yaghoubi F, Oroojalian F. Investigation and comparison of laser and ultrasound effects on the temperature increasing of the solutions containing graphene oxide nanoparticles for thermal treatment of osteosarcoma cancer cells. Nanomed J. 2023; 10(4): 313-322.
2. Taebpour M, Akhlaghi M, Shahriyari S, Hajihosseini S, Haghiralsadat BF, Oroojalian F, et al. Synthesis, physicochemical characterization and pharmaceutical function of niosomal nanoparticles-encapsulated bioactive compound for osteosarcoma treatment. Nanomed J. 2022; 9(3): 205-215.
3. Su Q, Xu B, Tian Z, Gong Z. 1,3,5-triazines inhibit osteosarcoma and avert lung metastasis in a patient-derived orthotopic xenograft mouse model with favorable pharmacokinetics. Iran J Basic Med Sci. 2022; 25(3): 295-301.
4. Kay CS, Kang Y. Curative radiotherapy in metastatic disease: how to develop the role of radiotherapy from local to metastases. Front Radiat Oncol. 2013; 3: 115.
5. Bao J, Zeng J, Song C, Yu H, Shi Q, Mai W, et al. A retrospective clinicopathological study of osteosarcoma patients with metachronous metastatic relapse. J Cancer. 2019; 10(13): 2982-2990.
6. Wang Z, Tian Y, Zhang H, Qin Y, Li D, Gan L, et al. Using hyaluronic acid-functionalized pH stimuli-responsive mesoporous silica nanoparticles for targeted delivery to CD44-overexpressing cancer cells. Int J Nanomedicine. 2016; 11: 6485-6497.
7. Abdelmoneem AM, Esser L, Wojnilowicz M, Voelcker NH. Surface-engineered porous silicon nanoparticles for targeted osteosarcoma therapy. Biomacromolecules. 2025; 26(8): 5020-5031.
8. Zhou Y, Wang S, Hu Y. Zinc oxide nanoparticle-reinforced sodium alginate/hydroxyapatite scaffolds for osteoporosis treatment in fragility fracture patients: development and characterization using artificial neural networks (ANNs) modeling. Iran J Basic Med Scie. 2024; 27(12): 1592-1603.
9. Hussain MA, Haq EU, Munawar I, Maqbool A, Saleem M, Rafiq MA, et al. Influence of spark plasma sintering temperature and hydroxyapatite nanoparticles on properties of HA based functionally graded materials for bone prosthesis. Ceram Int. 2022; 48(10): 14481-14490.
10. Asgharzadeh F, Hashemzadeh A, Eskandari M, Yaghoubi A, Naghibzadeh N, Mostafapour A, et al. Synthesis and evaluation of anti-inflammatory properties of hydroxyapatite nanoparticles in an experimental model of colitis. Nanomed J. 2022; 9(4): 319-327.
11. Zastulka A, Clichici S, Tomoaia-Cotisel M, Mocanu A, Roman C, Olteanu CD, et al. Recent trends in hydroxyapatite supplementation for osteoregenerative purposes. Materials (Basel). 2023; 16(3): 1303.
12. El-Bassyouni GT, Eldera SS, Kenawy SH, Hamzawy EMA. Hydroxyapatite nanoparticles derived from mussel shells for in vitro cytotoxicity test and cell viability. Heliyon. 2020; 6(6): e04085.
13. Fernandez de Grado G, Keller L, Idoux-Gillet Y, Wagner Q, Musset AM, Benkirane-Jessel N, et al. Bone substitutes: a review of their characteristics, clinical use, and perspectives for large bone defects management. J Tissue Eng. 2018; 9: 2041731418776819.
14. Cunha C, Sprio S, Panseri S, Dapporto M, Marcacci M, Tampieri A. High biocompatibility and improved osteogenic potential of novel Ca-P/titania composite scaffolds designed for regeneration of load-bearing segmental bone defects. J Biomed Mater Res A. 2012; 101(6): 1612-1619.
15. Wang X, Huang S, Peng Q. Metal ion-doped hydroxyapatite-based materials for bone defect restoration. Bioengineering. 2023; 10(12): 1367.
16. Tite T, Popa AB, Balescu LM, Bogdan IM, Pasuk I, Ferreira JMF, et al. Cationic substitutions in hydroxyapatite: current status of the derived biofunctional effects and their in vitro interrogation methods. Materials. 2018; 11(11): 2081.
17. Huang HL, Manga YB, Huang WR, Pakpour AH, Tseng CL, Huang HM, et al. Effect of hydroxyapatite formation on titanium surface with bone

morphogenetic protein-2 loading through electrochemical deposition on MG-63 cells. Materials. 2018; 11(10): 1897.
18. Beherei HH, Mohamed KR, El-Bassyouni GT. Mechanical and bioactivity properties of nano ceramic composite-based oxyapatite materials. Interceram Int Ceram Rev. 2014; 63(7): 386-392.
19. Liu J, Zhou Z, Hou M, Xia X, Liu Y, Zhao Z, et al. Capturing cerium ions via hydrogel microspheres promotes vascularization for bone regeneration. Mater Today Bio. 2024; 25: 100956.
20. Varini E, Sánchez-Salcedo S, Malavasi G, Lusvardi G, Vallet-Regí M, Salinas AJ. Cerium (III) and (IV) containing mesoporous glasses/alginate beads for bone regeneration: bioactivity, biocompatibility and reactive oxygen species activity. Mater Sci Eng C. 2019; 105: 109971.
21. Zhang L, Jiang H, Selke M, Wang X. Selective cytotoxicity effect of cerium oxide nanoparticles under UV irradiation. J Biomed Nanotechnol. 2014; 10(2): 278-286.
22. Wu Y, Ta HT. Different approaches to synthesising cerium oxide nanoparticles and their corresponding physical characteristics, and ROS scavenging and anti-inflammatory capabilities. J Mater Chem B. 2021; 9(36): 7291-7301.
23. Pramanik N, De T, Sharma P, Alakesh A, Jagirdar SK, Rangarajan A, et al. Surface-coated cerium nanoparticles to improve chemotherapeutic delivery to tumor cells. ACS Omega. 2022; 7(36): 31651-31657.
24. Priyadarshini B, Vijayalakshmi U. Development of cerium and silicon co-doped hydroxyapatite nanopowder and its in vitro biological studies for bone regeneration applications. Adv Powder Technol. 2018; 29(11): 2792-2803.
25. Gopi D, Sathishkumar S, Karthika A, Kavitha L. Development of Ce3+/Eu3+ dual-substituted hydroxyapatite coating on surgical grade stainless steel for improved antimicrobial and bioactive properties. Ind Eng Chem Res. 2014; 53(52): 20145-20153.
26. Astaneh ME, Noori F, Fereydouni N. Curcumin-loaded scaffolds in bone regeneration. Heliyon. 2024; 10(11): e32566.
27. Lotfi MS, Sheibani M, Jafari-Sabet M. Quercetin-based biomaterials for enhanced bone regeneration and tissue engineering. Tissue Cell. 2024; 91: 102626.
28. Gadkari PV, Balaraman M. Catechins: sources, extraction and encapsulation: a review. Food Bioprod Process. 2015; 93: 122-138.
29. Zanwar AA, Badole SL, Shende PS, Hegde MV, Bodhankar SL. Antioxidant role of catechin in health and disease. Polyphenols Hum Health Dis. 2014; 1: 267-271.
30. Manikandan R, Beulaja M, Arulvasu C, Sellamuthu S, Dinesh D, Prabhu D, et al. Synergistic anticancer activity of curcumin and catechin: an in vitro study using human cancer cell lines. Microsc Res Tech. 2011; 75(2): 112-116.
31. Jasmin I, Barbalho SM, Andreo JC, Lais T, Laurindo LF, Rodrigues VD, et al. Exploring the impact of catechins on bone metabolism: a comprehensive review of current research and future directions. Metabolites. 2024; 14(10): 560.
32. Huang HT, Cheng TL, Lin SY, Ho CJ, Chyu JY, Yang RS, et al. Osteoprotective roles of green tea catechins. Antioxidants. 2020; 9(11): 1136.
33. Baranwal A, Aggarwal P, Rai A, Kumar N. Pharmacological actions and underlying mechanisms of catechin: a review. Mini Rev Med Chem. 2022; 22(5):821-833.
34. Nicolin V, De Tommasi N, Nori SL, Costantinides F, Berton F, Di Lenarda R. Modulatory effects of plant polyphenols on bone remodeling: a prospective view from the bench to bedside. Front Endocrinol. 2019; 10: 494.
35. Checinska K, Checinski M, Cholewa-Kowalska K, Sikora M, Chlubek D. Polyphenol-enriched composite bone regeneration materials: a systematic review of in vitro studies. Int J Mol Sci. 2022; 23(13): 7473.
36. Carolina A, Borghesi J, Noratto GD. The role of dietary polyphenols in osteosarcoma: a possible clue about the molecular mechanisms involved in a process that is just in its infancy. J Food Biochem. 2021; 46(1): e14026.
37. Sinulingga K, Sirait M, Siregar N, Abdullah H. Synthesis and characterizations of natural limestone-derived nano-hydroxyapatite (HA): a comparison study of different metals doped HA on antibacterial activity. RSC Adv. 2021; 11(26): 15896-15904.
38. Shu K, Chuaicham C, Noguchi Y, Xu L, Sasaki K. In-situ hydrothermal synthesis of Fe-doped hydroxyapatite photocatalyst derived from converter slag toward xanthate photodegradation and Cr(VI) reduction under visible-light irradiation. Chem Eng J. 2023; 459: 141474.
39. Yu P, Sun K, Cheng C, Li H, Hu X, Yi Y, et al. Mitochondria-targeted cassic acid base nanoprodrug for enhanced anti-inflammatory and osteogenic effects in osteoarthritis. ACS Omega. 2025; 10(32): 35940-35953.
40. Joshi KJ, Shah NM. Structural, morphological & optical studies of hydroxyapatite microplates synthesized using hydrothermal technique. Mater Today Proc. 2023.
41. Yuan Q, Qin C, Wu J, Xu A, Zhang Z, Liao J, et al. Synthesis and characterization of cerium-doped hydroxyapatite/polylactic acid composite coatings on metal substrates. Mater Chem Phys. 2016; 182: 365-371.
42. Ciobanu G, Harja M. Cerium-doped hydroxyapatite/collagen coatings on titanium for bone implants. Ceram Int. 2019; 45(2): 2852-2857.
43. Zhao B, Deng S, Li J, Sun C, Fu Y, Liu Z. Green synthesis, characterization and antibacterial study on the catechin-functionalized ZnO nanoclusters. Mater Res Express. 2021; 8(2): 025006.
44. Lucida H, Hasani S, Susanti M, Ismed F. Formulation of a gambier catechin-loaded nanophytosome and the MTT assay on HeLa cell lines. Pharm Educ. 2023; 23(2): 19-24.
45. Li F, Jin H, Xiao J, Yin X, Liu X, Huang Q. The simultaneous loading of catechin and quercetin on

chitosan-based nanoparticles as effective antioxidant and antibacterial agent. Food Res Int. 2018; 111: 351-360.
46. Singh R, Manna PP. Reactive oxygen species in cancer progression and its role in therapeutics. Explor Med. 2022; 3(1): 43-57.
47. Wang Y, Nartiss Y, Steipe B, McQuibban GA, Kim PK. ROS-induced mitochondrial depolarization initiates PARK2/PARKIN-dependent mitochondrial degradation by autophagy. Autophagy. 2012; 8(10): 1462-1476.
48. Xiong S, Mu T, Wang G, Jiang X. Mitochondria-mediated apoptosis in mammals. Protein Cell. 2014; 5(10): 737-749.
49. Marsden VS, Ekert PG, Van Delft M, Vaux DL, Adams JM, Strasser A. Bcl-2-regulated apoptosis and cytochrome c release can occur independently of both caspase-2 and caspase-9. J Cell Biol. 2004; 165(6): 775-780.
50. Xie X, Shi X, Wang S, Cao L, Yang C, Ma Z. Effect of attapulgite-doped electrospun fibrous PLGA scaffold on pro-osteogenesis and barrier function in the application of guided bone regeneration. Int J Nanomedicine. 2020; 15: 6761-6777.